PHYSICAL REVIEW A **66**, 051404(R) (2002)

Electron diffraction in above-threshold ionization of molecules

M. Lein,* J. P. Marangos, and P. L. Knight
Blackett Laboratory, Imperial College of Science, Technology and Medicine, London SW7 2BW, United Kingdom
(Received 5 July 2002; published 19 November 2002)

We calculate the spectra and angular distributions of electrons from ionization of two-center molecules in linearly polarized strong laser pulses. A fully numerical quantum-mechanical method is compared to a simple semiclassical model designed to describe the diffraction of electrons when they recollide with the two-center core. Within both approaches, clear signatures of diffraction are found in the angular distributions. We discuss the dependence of electron diffraction on the internuclear distance and on the molecular orientation.

DOI: 10.1103/PhysRevA.66.051404 PACS number(s): 33.80.Rv, 34.80.Bm

When an atom or molecule is ionized by an intense laser pulse, more photons than necessary to overcome the ionization threshold are typically absorbed. This process is called above-threshold ionization (ATI) [1,2], and results in photoelectron spectra consisting of peaks separated by the photon energy. The spectral envelope is divided into two regions: small electron energies correspond to electrons that are ejected without further interaction with the core (''direct electrons''). Beyond the energies of direct electrons, a plateau extends up to energies of $10U_p$ [3–5], where U_p is the ponderomotive potential. These electrons are due to rescattering: electrons can scatter elastically from the core after they are driven back by the laser field. After the recollision, the scattered electron is further accelerated by the field and can thus gain a large amount of energy. There has been no systematic study of the plateau structure for molecules. However, it has been suggested that scattering from more than one nucleus gives rise to a diffraction pattern in the electron angular distribution [6], because the wave packets scattered from different nuclei can interfere constructively or destructively with each other. A change in the molecular geometry would then lead to a change in the electron distribution, so that ATI could be used as a tool to probe nuclear dynamics.

Two related interference effects were recently found: ionization of the O_2 molecule is suppressed due to destructive interference arising from the antibonding symmetry of the valence orbital [7,8]. Furthermore, interference structures in high-harmonic generation (HHG) [9,10] were shown to originate from the constructive or destructive superposition of radiation emitted at different atomic sites. Similar to the electron diffraction expected in high-order ATI, the HHG interference effect comes from the quantum nature of the recolliding electrons, while the suppression of ionization in O_2 is due to the interference of the electron waves emitted from the two atomic sites without rescattering.

In this paper we calculate the energy spectra and angular distributions of ATI electrons from two-center molecules in linearly polarized light. This is achieved by numerical solution of the Schrödinger equation for a two-dimensional H_2^+ model molecule at various angles between molecule and field. ATI in 1D H_2^+ has been investigated in the past [11], but with respect to low-order photon absorption in the UV regime. We compare our results to the predictions of an intuitive semiclassical model in order to make evident which features are due to the diffraction of recolliding electrons. Also, we briefly compare interference effects in ATI and HHG.

The numerical treatment of ATI is a difficult task because it must keep track of electrons traveling far away from the nucleus. A grid containing the entire electron wave function would need to span thousands of atomic units because the wave packets spread rapidly after ionization. To keep the computational effort manageable, we apply a method similar to one that was previously used in the calculation of electron spectra for intense-field double ionization [12]. We divide the configuration space into two parts I and II with wave functions Ψ_I and Ψ_{II} such that the total wave function is $\Psi = \Psi_I + \Psi_{II}$. Part I is the inner region, where the electron is close to the nucleus. In this region, the wave function is propagated as prescribed by the time-dependent Schrödinger equation for an electron in a potential $V(\mathbf{r})$ driven by an electric field $E(t)$ polarized along the x axis,

$$i\frac{\partial \Psi_I(\mathbf{r},t)}{\partial t} = \left(\frac{\mathbf{p}^2}{2} + p_x A(t) + V(\mathbf{r})\right)\Psi_I(\mathbf{r},t), \tag{1}$$

where $A(t) = -\int_0^t E(t')dt'$. (Atomic units are used throughout.) The propagation is achieved by means of the split-operator method [13]. Part II is the outer region where the electron is far away from the nucleus. Here, the interaction between core and electron is neglected. The Schrödinger equation then becomes

$$i\frac{\partial \Psi_{II}(\mathbf{p},t)}{\partial t} = \left(\frac{\mathbf{p}^2}{2} + p_x A(t)\right)\Psi_{II}(\mathbf{p},t), \tag{2}$$

and the propagation of the wave function is simply accomplished by multiplications in momentum space. The inner region has an absorbing boundary. The absorbed portion of the wave function Ψ_I, however, is not discarded, but Fourier transformed and coherently added to the wave function Ψ_{II} which is represented in momentum space at all times. The flux information about outgoing electrons is thus collected in part II. Typically, we take part I to be a rectangle of size 1106×369 a.u. where the larger value is for the direction parallel to the electric field. Then, the value of $|V(\mathbf{r})|$ along the boundary of part I is below 0.011 a.u. which is negligible compared to the typical electron quiver energy in part II

*Present address: Max Planck Institute for the Physics of Complex Systems, Nöthnitzerstraβe 38, D-01187 Dresden, Germany.

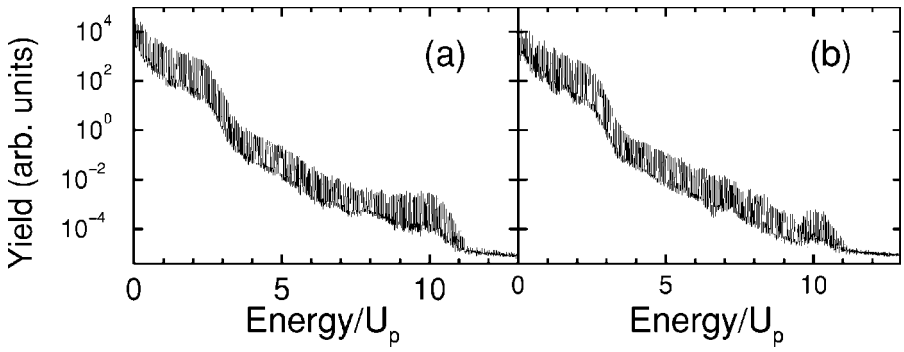

FIG. 1. ATI spectrum for a 780-nm laser pulse with intensity 5×10^{14} W/cm^2 acting on the model H_2^+ molecular ion at $R=2$ a.u. aligned (a) parallel or (b) perpendicular to the field.

($U_p=1.04$ a.u., see below.) The absorbing mask is applied 32 times per optical cycle. The width of the absorber is 111 a.u. in x direction with a $\sin^{2/3}$-shaped mask, and 46 a.u. in the perpendicular direction with a $\sin^2$-shaped mask. The absorption is thus very smooth and reflections from the boundary are negligible. With a spatial grid-point separation of 0.36 a.u., the representable momenta extend from -8.73 to $+8.73$ a.u. in each component of the momentum vector. This is also the size of the momentum-space grid in the outer part II. At the end of the propagation, the photoelectron spectrum is obtained from the final wave function in part II.

We employ trapezoidally shaped 10-cycle laser pulses with 3-cycle linear ramps, 780 nm wavelength and 5×10^{14} W/cm^2 intensity. The momentum of a free electron oscillates with the amplitude $E_0/\omega=2.04$ a.u. (Here, E_0 is the peak field strength, and ω is the laser frequency.) Adding the drift momentum 4.57 a.u. of an electron with $10U_p$ energy gives $p_{max}=6.61$ a.u. as a classical estimate for the largest possible momentum. This is easily represented on our numerical grid. After the end of the pulse, the wave function is propagated without field for an additional time of six optical cycles. In this way, all electrons with energies above 0.36 a.u.$=9.8$ eV are collected in part II while electrons with smaller energies are at least partially collected.

As binding potential we use the two-center soft-Coulomb potential which was used in Refs. [14,9] as a model potential for H_2^+. Unless stated otherwise, calculations are performed for the equilibrium internuclear distance $R=2$ a.u. These calculations are not expected to reproduce experiments on real H_2^+ ions, because ionization of real H_2^+ is dominated by charge resonance enhanced ionization at internuclear separations much larger than the equilibrium bondlength [15]. The model is, however, suitable to describe many features of the ionization of neutral molecules which usually occurs near the ground-state geometry.

Figure 1 shows the ATI spectra for parallel and perpendicular orientation of the molecule relative to the field. The electron energy is given in units of the ponderomotive potential which is defined as $U_p=E_0^2/(4\omega^2)$. For the present laser parameters, we have $U_p=1.04$ a.u.$=28.4$ eV. For both orientations, we obtain the typical features previously found for atomic ATI spectra. The first plateau reaching up to about $2.5U_p$ comes from the direct electrons. The scattered electrons give rise to the second plateau between $3U_p$ and $10U_p$. Each of the spectra consists of nearly 200 well-defined ATI peaks. The only major differences between the two orientations are the local minimum at $9.5U_p$ for perpendicular orientation and the higher yield for parallel orientation; the overall ratio of yields is 1.6.

Before we present further results, we introduce a semiclassical model that contains the essential physics of rescattering in high-order ATI of molecules. The model is an extension of the classical model of Ref. [4], which was able to reproduce the side lobes in the angular distribution of atomic ATI spectra. Our model describes the kinematics of recolliding electrons classically as in Ref. [4], but includes the interference of electron waves scattered from different atomic centers. We assume that the internuclear distance is small enough so that a single wave packet is formed in the event of ionization rather than two spatially separated wave packets. More precisely, this approach is applicable if the transverse spread of a recolliding wave packet is larger than the internuclear distance. The classical equation of motion for an electron in a monochromatic field is $\ddot{x}=-E_0\sin\omega t$. If ionization occurs at the phase ϕ of the field and creates an electron with initial velocity zero at $x=0$, this electron will return to the origin after the travel time τ if τ is a solution to

$$(\omega\tau-\sin\omega\tau)\cos\phi=(\cos\omega\tau-1)\sin\phi. \tag{3}$$

The electron returns with an impact velocity of

$$\dot{x}_r=(E_0/\omega)(\cos\phi'-\cos\phi), \tag{4}$$

where $\phi'=\omega\tau+\phi$ is the phase of the field at the time of return. If the molecule with internuclear distance R is oriented at an angle θ relative to the field, the returning electron wave packet hits the two nuclei with a phase difference of $\varphi_1=\dot{x}_r R\cos\theta$. We assume that the returning electron is scattered by an angle ϑ_0 in the (x,y) plane which is the plane spanned by the molecule and the laser polarization axis [16]. Then the electron leaves with the final velocity components

$$\dot{x}_f=(E_0/\omega)\,[\cos\vartheta_0(\cos\phi'-\cos\phi)-\cos\phi'], \tag{5}$$

$$\dot{y}_f=(E_0/\omega)\,\sin\vartheta_0(\cos\phi'-\cos\phi). \tag{6}$$

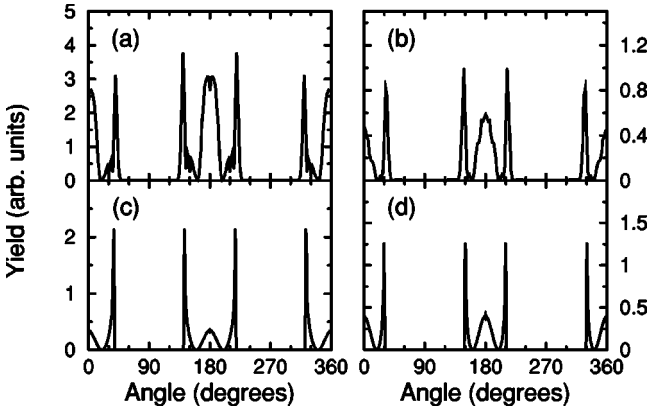

FIG. 2. Angular distribution of ATI electrons for the parameters of Fig. 1(b) (perpendicular alignment of H_2^+). (a) and (b) show quantum-mechanical results for electron energies of $7U_p$ and $8U_p$, respectively. (c) and (d) are the results of the semiclassical model.

The phase difference φ_2 due to the emission of electron waves at two different positions is

$$\varphi_2 = -\dot{x}_r R(\cos\vartheta_0 \cos\theta + \sin\vartheta_0 \sin\theta). \tag{7}$$

Owing to the attractive Coulomb tail of the molecular potential, the electron impact velocity is actually larger than given by Eq. (4). This can approximately be taken into account by assuming that the electron kinetic energy increases by the ionization potential I_p. Since the velocity is proportional to the square root of the energy, we multiply the total phase difference by a correction factor

$$\alpha = \sqrt{(T+I_p)/T}, \tag{8}$$

where $T=\dot{x}_r^2/2$ is the uncorrected impact kinetic energy from Eq. (4). The resulting total phase difference $\varphi=\alpha(\varphi_1+\varphi_2)$ for two-center scattering is then

$$\varphi = -\alpha((E_0/\omega)\cos\phi + \dot{x}_f)R\cos\theta - \alpha\dot{y}_f R\sin\theta. \tag{9}$$

Each electron trajectory gives a contribution proportional to $|1+\exp(i\varphi)|^2 = 4\cos^2(\varphi/2)$. Assuming a uniform distribution of ionization times and scattering angles, and ignoring multiple returns of electrons, we can calculate the angular distribution of photoelectrons. In general, there are two distinct trajectories (corresponding to two different phases φ) leading to the same final electron momentum vector. Therefore, we do not normally encounter perfect destructive or constructive interference except in the case of perpendicular alignment ($\theta=90°$), where we have the simple relationship

$$\varphi = -\alpha\dot{y}_f R. \tag{10}$$

Figure 2 shows the angular distributions of ATI electrons for perpendicular alignment. The panels on the left-hand side are for electrons of $7U_p=199$ eV energy, the right-hand side is for electrons at $8U_p=227$ eV. In each case, we have integrated over an energy interval covering three ATI peaks. We find good agreement between the quantum-mechanical results (upper panels) and the semiclassical results (lower panels). The distributions are centered around the laser polarization axis, i.e., around 0° and 180°. As familiar from atomic distributions, the width decreases with increasing electron energy. The semiclassical model predicts four angles of complete destructive interference, their locations depending only slightly on the electron energy: 20°, 160°, 200°, 340° for $7U_p$ and 19°, 161°, 199°, 341° for $8U_p$. These positions agree well with the quantum-mechanical results.

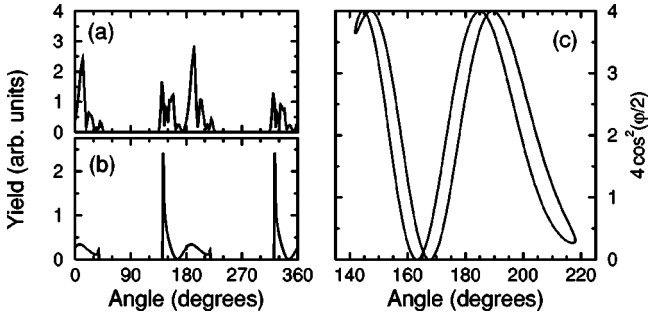

FIG. 3. Left: Angular distribution of ATI electrons at $7U_p$ for the H_2^+ molecule aligned at $\theta=60°$ relative to the polarization axis. (a) Quantum-mechanical results. (b) Semiclassical model. Right: Interference term at $\theta=60°$.

For atoms, it was shown that the quantum-mechanical angular distributions are qualitatively different from the classical distributions, in the sense that quantum mechanically, there are always local maxima at 0° and 180° [17], which are not reproduced by the classical model [4]. For the same reason our semiclassical model gives a systematic underestimate of emission along the polarization axis in the case of molecules.

For orientations other than $\theta=90°$, the agreement between the quantum-mechanical results and the semiclassical model is also reasonable. This can be seen in Figs. 3(a) and 3(b), where we show the angular distribution of electrons at $7U_p$ energy for $\theta=60°$. Interestingly, we still find a clear interference structure, although there is no perfect constructive or destructive interference. This is evident from a plot of the interference term $4\cos^2(\varphi/2)$ versus emission angle, see Fig. 3(c). Within the classically allowed range of emission angles, there are two possible trajectories for every angle, associated with two different phases φ. Consequently, there are two sets of interference extrema which are in general shifted with respect to each other. In Fig. 3, the shift is small, so that the diffraction pattern remains intact.

With increasing internuclear distance R, the diffraction extrema move closer together while the angular range covered by the distributions remains the same. This behavior—which is characteristic of diffraction—is shown in Fig. 4 where we compare $R=5$ a.u. and $R=10$ a.u. for an alignment angle of $\theta=45°$. The overall width of the diffraction pattern is always determined by the classically allowed range of emission angles, see Fig. 3(c), and thus independent of the internuclear distance.

A peak in the ATI spectrum, Fig. 1, can be understood as the integral over its angular distribution. Since a typical angular distribution exhibits both interference minima and maxima, we do not expect that the intensity of an ATI peak

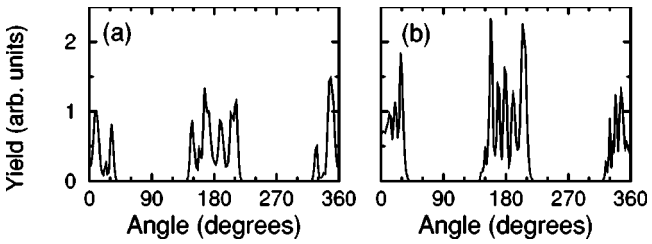

FIG. 4. Angular distributions of ATI electrons at $8U_p$ energy for the H_2^+ molecule aligned at $\theta=45°$ with an internuclear distance of (a) 5 a.u., (b) 10 a.u. (quantum-mechanical results).

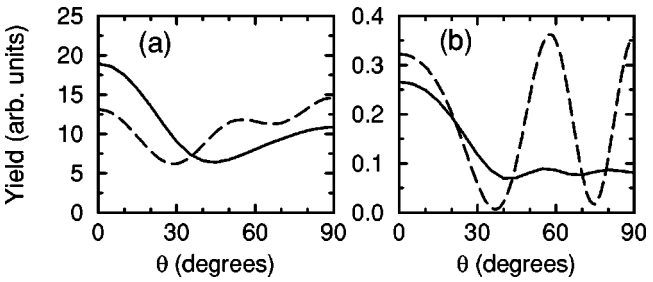

FIG. 5. Intensity of the ATI peaks at (a) $5U_p$ and (b) $10U_p$ vs molecular orientation. Solid lines, quantum-mechanical results. Dashed lines, semiclassical model (arbitrary scale).

can be maximized or minimized due to two-center interference. An exception, however, is the upper end of the ATI spectrum at $10U_p$. Classically, the highest electron energy is produced by only one trajectory, more specifically one, where the electron is backscattered from the core by 180°. Figure 5(b) shows the intensity of the ATI peak closest to $10U_p$ versus the orientation of the molecule. The semiclassical model predicts a clear interference pattern with minima at 37° and 75°. Numerically, we find that the effect of interference is much weaker, and the minima appear at the slightly shifted positions 42° and 68°. Figure 5(a) is for the lower energy $5U_p$. Here, quantum and semiclassical results largely disagree. This indicates that the orientation dependence is dominated by effects other than the two-center interference. From Fig. 5, we also infer that the semiclassical model does not explain the differences between the ATI spectra obtained for parallel and perpendicular alignment, Fig. 1. These effects remain to be investigated in future work.

Previously, the conditions for constructive and destructive interference in molecular HHG were shown to be rather simple and independent of the laser parameters [10]. For example, constructive interference occurs when the projection of the internuclear distance onto the polarization axis $R\cos\theta$ equals an integer multiple of the wavelength of the recolliding electron λ, which is related to the energy of the emitted photon E_{ph} by $k^2/2=E_{ph}$ with $k=2\pi/\lambda$. Clearly, the interference conditions in high-order ATI are more complicated since they depend on the laser parameters through the term $(E_0/\omega)\cos\phi$ in Eq. (9). Therefore, if one aims at using interference effects as a probe of nuclear dynamics, it could be more appropriate to use HHG rather than ATI. On the other hand, since angular distributions can be measured for various electron energies, ATI provides a larger amount of data that one can analyze.

In summary, we have analyzed high-order ATI of a model two-center molecule in linearly polarized light. The diffraction of electrons when they recollide with the molecular core gives rise to an interference pattern in the angular distribution of high-order ATI electrons. For electrons near the cutoff, interference structures are found also in the orientation dependence of the ionization yield. In contrast to HHG, the conditions for constructive and destructive interference depend on the laser parameters. Future calculations and experiments will have to decide whether ATI or HHG can be efficiently used as a tool to probe nuclear dynamics.

This work was supported by the UK Engineering and Physical Sciences Research Council, and by the EU "COCOMO" network (Grant No. EU-IHP HPRN-CT-1999-0129).

[1] P. Agostini, F. Fabre, G. Mainfray, G. Petite, and N.K. Rahman, Phys. Rev. Lett. **42**, 1127 (1979).
[2] J.H. Eberly, J. Javanainen, and K. Rzążewski, Phys. Rep. **204**, 331 (1991).
[3] G.G. Paulus *et al.*, Phys. Rev. Lett. **72**, 2851 (1994).
[4] G.G. Paulus, W. Becker, W. Nicklich, and H. Walther, J. Phys. B **27**, L703 (1994).
[5] G.G. Paulus, W. Becker, H. Walther, Phys. Rev. A **52**, 4043 (1995).
[6] H. Niikura *et al.*, Nature (London) **417**, 917 (2002).
[7] J. Muth-Böhm, A. Becker, and F.H.M. Faisal, Phys. Rev. Lett. **85**, 2280 (2000).
[8] F. Grasbon *et al.*, Phys. Rev. A **63**, 041402 (2001).
[9] M. Lein, N. Hay, R. Velotta, J.P. Marangos, and P.L. Knight, Phys. Rev. Lett. **88**, 183903 (2002).
[10] M. Lein, N. Hay, R. Velotta, J.P. Marangos, and P.L. Knight, Phys. Rev. A **66**, 023805 (2002).
[11] A.D. Bandrauk and S. Chelkowski, Phys. Rev. Lett. **87**, 273004 (2001).
[12] M. Lein, E.K.U. Gross, and V. Engel, Phys. Rev. Lett. **85**, 4707 (2000); Phys. Rev. A **64**, 023406 (2001).
[13] M.D. Feit, J.A. Fleck, Jr., and A. Steiger, J. Comput. Phys. **47**, 412 (1982).
[14] D.G. Lappas and J.P. Marangos, J. Phys. B **33**, 4679 (2000).
[15] T. Zuo and A.D. Bandrauk, Phys. Rev. A **52**, R2511 (1995); T. Seideman, M.Y. Ivanov, and P.B. Corkum, Phys. Rev. Lett. **75**, 2819 (1995).
[16] In order to compare with the 2D quantum calculations, the semiclassical results were obtained for 2D geometry. The generalization of the model to 3D is obvious. We found that 3D semiclassical calculations give angular distributions in the (x,y) plane almost identical to the 2D ones. The quantum calculation in 3D, however, is beyond the scope of this work.
[17] W. Becker, A. Lohr, and M. Kleber, J. Phys. B **27**, L325 (1994).